Energetic and Entropic Forces Governing the Attraction between Polyelectrolyte-Grafted Colloids

Gaurav Arya*

Department of Nanoengineering, University of California, San Diego, 9500 Gilman Drive, Mail Code: 0448, La Jolla, California 92093

Received: August 19, 2009; Revised Manuscript Received: September 25, 2009

The energetic and entropic interactions governing the attraction between like-charged colloidal particles grafted with oppositely charged polyelectrolyte chains in a monovalent electrolyte are investigated computationally. We employ coarse-grained models of the colloids with varying surface and polyelectrolyte charges and Monte Carlo simulations to compute the potential of mean force between two colloidal particles as a function of their separation distance. By categorizing the potentials as attractive or purely repulsive, we obtain the extent and location of the attractive-force regime within the two-dimensional parameter space comprised of the colloid surface and polyelectrolyte charge. The attractive regime is found to occupy the inside of a hyperbola in this charge space, whose shape and size is determined by a complex interplay between energetic and entropic interactions. In particular, we find that the strength of attraction at short distances is governed by a balance between favorable energetic and entropic terms arising from polymer-bridging interactions, unfavorable energies arising from the mutual repulsion of the colloid surfaces and polyelectrolyte chains, and unfavorable entropies arising from the overlap and crowding effects of chains confined between the colloid surfaces. A phenomenological model is proposed to explain the hyperbolic shape of the attractive regime and make useful predictions about changes in its shape and location for conditions not investigated in this study.

1. Introduction

Polyelectrolyte-grafted colloidal particles in which the polyelectrolyte chains and the colloid surface carry charges of opposite signs are important systems to study because of their numerous industrial applications[1] and interesting physical properties. A particularly interesting property is that these colloidal particles could exhibit a mutual attraction under certain conditions, despite the *likeness* in their overall charge, resulting in their phase separation or flocculation.[2,3] Perhaps the best example of such an attraction occurs inside our cells, where histone protein−DNA complexes called nucleosomes containing a highly negatively charged core (colloid) and several positively charged floppy histone domains extending outward (polyelectrolyte chains) exhibit an overall attractive interaction despite their overall strong negative charge.[4−7]

The primary driving force for this attraction is the so-called "polymer-bridging" effect, where polyelectrolyte chains from one colloidal particle get adsorbed onto the oppositely charged surface of another particle to form an attractive elastic bridge that can sometimes surpass the mutual repulsion between the chains and the colloid surfaces. Correlations between charges on opposite particles, analogous to correlations between electrons in van der Waals interactions, could also result in a net attraction between colloidal particles. However this attraction is expected to be weaker and more short-ranged compared to that from polymer-bridging attraction.[7] Polymer-bridging attraction is also observed between charged surfaces when the polyelectrolyte chains are mobile in solution (not grafted). In fact, the first polymer-bridging hypothesis was proposed to explain flocculation observed in such systems.[8] Since then, several theoretical studies have examined this attraction in more detail that generally fall into two main categories: mean-field theory and molecular simulations.

In the mean-field approach,[9,10] the many-body interactions between chains, counterions, and surfaces are replaced by a "mean" field and the resulting equations are solved self-consistently to yield the spatially dependent polymer density that minimizes the total free energy. The first evidence[11] that polymer bridging could lead to an attraction came from the application of such a theory to a single charged polymer confined between charged plates. Since then, this approach has been extended to treat multiple chains and other effects such as excluded volume,[12,13] steric and van der Waals interactions,[13,14] grafted polyelectrolytes,[15,16] spherical and cylindrical geometries,[15,17] and multibody systems.[17] An alternative mean-field theory based on the extension of the Poisson−Boltzmann (PB) equation to cases where the mobile point-charge counterions are now connected by bonds to represent the polyelectrolyte was also proposed to explain the origin of bridging attraction.[18] This theory has also been extended to investigate polyelectrolyte-grafted surfaces.[19]

In molecular simulations, Monte Carlo (MC) and molecular dynamics (MD) methods are used to generate Boltzmann-distributed configurations of the colloidal particles whose intra- and intermolecular intractions are treated via atomistic or coarse-grained force fields. Akesson et al.[18] used MC simulations to provide evidence for attraction between like-charged surfaces confining short mobile polyelectrolyte chains treated as point charges connected by harmonic springs. Other studies have also demonstrated attraction between like-charged surfaces grafted with polyelectrolyte chains.[19] A similar attraction was observed when the polyelectrolyte chains grafted on one of the surfaces were removed and replaced by mobile ions of the same charge.[20] In all of these studies, the medium was free of counterions. Other simulations on like-charged spherical colloids carrying

* To whom correspondence should be addressed. E-mail: garya@ucsd.edu. Phone: 858-822-5542. Fax: 858-534-9553.

10.1021/jp908007z CCC: $40.75
Published on Web 10/20/2009

adsorbed polyelectrolytes in an electrolyte also revealed attraction despite electrostatic screening, albeit at a reduced strength.[21] Some simulation studies have also examined the effect of chain length[22] and flexibility[23] on the attraction strength. A number of simulation studies have also specifically addressed the attraction between nucleosome core particles and shown that they aggregate in monovalent and divalent salt[24] and that polymer-bridging interactions are the main contributor to this attraction.[7]

Though the above studies have provided many important insights into attraction in polyelectrolyte-grafted colloids, several aspects of it remain unresolved. One important issue that has not been addressed in detail is the dependence of the attractive force on the colloid surface and polyelectrolyte charges. Previous studies have examined very specific systems and a narrow range of surface and polyelectrolyte charge values, often examining the effect of one charge keeping the other fixed, leading to conflicting results. For example, Miklavic et al.[19] used PB theory and MC simulations to show that the attraction between two polyelectrolyte-grafted surfaces for an overall electroneutral system increases monotonically with surface charge. Huang and Ruckenstein[14] used a mean-field theory for polyelectrolyte coated surfaces to show that the attraction increases with the polyelectrolyte charge. On the other hand, Granfeldt et al.,[21] using MC simulations, and Podgornik,[12] using a mean-field theory, observed a nonmonotonic dependence of the attractive force with the surface charge for adsorbed polyelectrolyte on charged surfaces. Evidently, the attractive force between polyelectrolyte-grafted colloids has a nontrivial dependence on the surface and polyelectrolyte charges, and a more careful examination of this is required.

Another unresolved issue concerns the contribution of energy and entropy to the overall free energy of interaction between two colloidal particles, which could explain the complex charge dependence described above. It is anticipated that a loss in energy should accompany polymer bridging. However, it is not so clear if polymer bridging could also contribute an entropic driving force for attraction. One would expect that the strong adsorption of the grafted polyelectrolyte chain onto the apposing surface would restrict its freedom, thus contributing an unfavorable entropy term to the overall free energy. However, the bridging interactions could also lead to a favorable entropic gain. Consider a polyelectrolyte chain strongly adsorbed on its own surface. The presence of another attractive surface nearby could promote the chain's detachment, allowing it to attach to both surfaces. We expect that such effects, as well as repulsion from the overlap of polyelectrolyte chains, are strongly dependent on the chain stiffness and length, and on the surface and polyelectrolyte charges. A systematic investigation of such an interplay between various energetic and entropic interactions has not been carried out so far.

Here, we use molecular simulations to provide key insights about the attraction between polyelectrolyte-grafted colloids and its dependence on surface and polyelectrolyte charges in terms of detailed energetics. Specifically, we employ coarse-grained models and MC simulations to compute the potential of mean force (PMF) between two colloidal particles as a function of their separation distance. By categorizing the PMFs as attractive or repulsive, we determine the extent of the attractive-force regime within a broad two-dimensional space of surface and polyelectrolyte charges. By further decomposing the PMF into energetic and entropic contributions, we quantify their role in the observed attraction between polyelectrolyte-grafted colloids and the shape of the attractive regime in the charge space. The methodological framework introduced here could be used to investigate the effect of other important parameters such as the grafting density, length, and flexibility of the polyelectrolyte chains on colloid attraction, and to study other related systems.

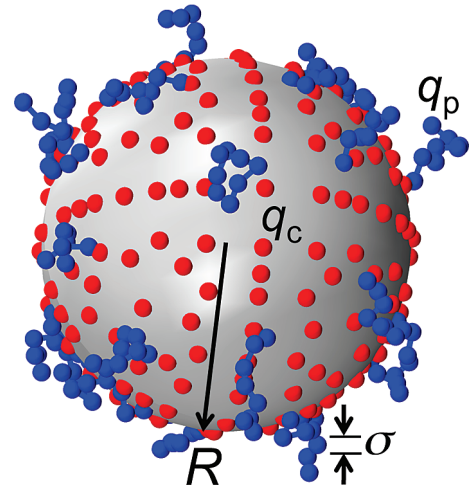

Figure 1. Coarse-grained model of a polyelectrolyte-grafted colloidal particle. The polyelectrolyte chain beads are shown in blue, and the surface charges are shown in red. The excluded volumes associated with the charges are not drawn to scale.

2. Methods

2.1. Coarse-Grained Modeling of Colloids. The polyelectrolyte-grafted colloids are treated using the coarse-grained model in Figure 1. The colloid is treated as a sphere of radius R carrying $n_c = 250$ charges, each of magnitude $q_c > 0$, scattered uniformly on the surface using the Marsaglia algorithm.[25] Hence, the colloid surface carries a total charge of $Q_c = n_c q_c$. Such a discrete representation of surface charge over a continuous one using surface densities allows us to simultaneously treat charge and excluded volume effects. The colloid is also grafted with $n_p = 26$ polyelectrolyte chains carrying the opposite charge. Each chain is modeled as a chain of $N = 8$ coarse-grained beads, where each bead carries a charge of $q_p < 0$. The total charge carried by the grafted chains is therefore given by $Q_p = N n_p q_p$. The surface charges are rigidly attached to the colloid, while the polyelectrolyte chains are modeled flexibly.

The total energy of interaction between two colloidal particles, U_{tot}, is given by the sum of electrostatic (U_{el}), excluded volume (U_{ev}), and intramolecular bonded energies (U_{intra}):

$$U_{tot} = U_{el} + U_{ev} + U_{intra} \quad (1)$$

We consider that the particles are present in a 1:1 electrolyte (monovalent salt). Therefore, all electrostatic interactions are treated using the Debye−Hückel formulation,[26] i.e., charges q_i and q_j separated by a distance r_{ij} interact through the Debye−Hückel potential:

$$U_{el}(d) = \sum_{i,j>i} \frac{q_i q_j}{4\pi\varepsilon\varepsilon_0 r_{ij}} \exp(-\kappa r_{ij}) \quad (2)$$

where the sum i, j runs over all surface and polyelectrolyte charges, ε_0 is the permittivity of the vacuum, ε is the dielectric constant of water. The inverse Debye length κ is given by $(2e^2 c_s/\varepsilon\varepsilon_0 k_B T)^{1/2}$, where e is the electronic charge, k_B is the Boltzmann constant, T is the temperature, and c_s is the salt concentration.

TABLE 1: Parameter Values for Our Coarse-Grained Model of Grafted Colloid

parameter	description	value
R	radius of colloid	10 nm
n_p	number of polyelectrolyte chains attached to core	26
N	number of beads composing each polyelectrolyte chain	8
n_c	number of charges on colloid surface	250
l_0	equilibrium segment length of polymer	1 nm
θ_0	equilibrium angle between three chain beads	180°
k_s	stretching constant of chains	10 kcal/mol/nm^2
k_θ	bending constant of chains	0.1 kcal/mol/rad^2
ϵ	LJ energy parameter for all excluded volume interactions	0.1 kcal/mol
σ_{cc}	LJ size parameter for surface charge interactions	1.2 nm
σ_{tc}	LJ size parameter for chain bead/surface charge interactions	1.8 nm
σ_{tt}	LJ size parameter for chain bead interactions	1.8 nm
ε	dielectric constant of solvent	80
c_s	electrolyte concentration	22 mM
κ	Inverse Debye length	0.5 nm^{-1}
T	temperature	293.15 K

Charges on the same surface and beads on the same chain i and j closer than three beads ($j - i < 3$) do not interact with each other.

Excluded volume interactions between colloid charges and polyelectrolyte beads are treated using the Lennard-Jones potential, as given by

$$U_{ev}(d) = \sum_{i,j>i} 4\epsilon_{ij}\left[\left(\frac{\sigma_{ij}}{r_{ij}}\right)^{12} - \left(\frac{\sigma_{ij}}{r_{ij}}\right)^{6}\right] \quad (3)$$

where the sum i, j runs over all surface charges and polyelectrolyte beads, σ_{ij} is the size parameter, and ϵ_{ij} is the well-depth of the potential. Similar to the electrostatic interactions, charges on the same surface and beads on the same chain i and j closer than three beads do not interact with each other via excluded volume interactions.

Each polyelectrolyte chain is assigned an intramolecular force field comprised of harmonic stretching and bending terms. In addition, a harmonic spring is used to attach the chains to the colloid surface at specific points $\mathbf{r}_{i0}$ to yield a uniformly grafted colloid (see Figure 1). The total intramolecular bonded energy for a single chain is therefore given by

$$U_{intra}(d) = \sum_i (k_s|\mathbf{r}_{i1} - \mathbf{r}_{i0}|^2 + \sum_{j=1}^{N-1} k_s(l_{ij} - l_0)^2 + \sum_{j=1}^{N-2} k_\theta(\theta_{ij} - \theta_0)^2) \quad (4)$$

where the sum i runs over all chains in the two-particle system, k_s and k_θ are the stretching and bending constants, respectively, $\mathbf{r}_{i1}$ is the position of the bead attached to the surface, l_{ij} is the bond length between beads j and $j + 1$, θ_{ij} is the bond angle between beads j, $j + 1$, and $j + 1$, and l_0 and θ_0 are the equilibrium bond lengths and angles.

The parameters related to this model are provided in Table 1. They have been chosen to be as realistic as possible, keeping computational demands in mind. In particular, ϵ_{ij} describing the depth of the van der Waals energy well has been kept small ($\ll k_BT$) so that it does not affect the final attraction between the two colloidal particles, as the main focus of this article is on electrostatic interactions. Also, we have fixed the salt concentration c_s to 22 mM so that it yields a characteristic Debye layer of thickness ~2 nm, on the order of the dimensions of the chains.

2.2. Potential of Mean Force Calculations. To determine the "effective" interaction between two colloidal particles, we compute the potential of mean force (PMF) as a function of their separation distance d defined as the distance between the colloid centers. The PMF is essentially a free energy of the system where the two particles are constrained to be a specific distance apart but are free to sample their remaining degrees of freedom such as colloid angular orientation and chain configuration. Hence, the PMF is a more accurate indicator of effective interaction between particles, as it contains contributions from both the energy and entropy. In this study, we compute the PMF by first computing the average force ($F(d)$) experienced by two particles in the direction along the particle centers through proper averaging over the remaining degrees of freedom:

$$\langle F(d)\rangle = \int \ldots \int -\left(\frac{\partial U_{tot}(d, \mathbf{\Omega})}{\partial d}\right) \exp(-U_{tot}(d, \mathbf{\Omega})/k_BT)\, d\mathbf{\Omega} \quad (5)$$

where U_{tot} is the total energy computed from eqs 1−4 and the integral is computed over all degrees of freedom represented collectively by $\mathbf{\Omega}$.

To compute $\langle F(d)\rangle$, we generate Boltzmann-distributed configurations of the two colloids subject to the distance constraint using a Monte Carlo approach consisting of two moves: rotation and chain regrowth. In the rotation move, one of the two colloidal particles is randomly chosen and rotated about a randomly picked axis. The colloid particle along with the grafted polyelectrolyte chains is then rotated by a random angle $\Delta\theta$ sampled from a uniform distribution $-45° < \Delta\theta < 45°$. The move is accepted using the standard Metropolis acceptance criterion:

$$p_{acc} = \min[1, \exp(-\Delta U_{tot}/k_BT)] \quad (6)$$

where ΔU_{tot} is the change in the total energy upon rotation. In the regrowth move, a polyelectrolyte chain is randomly chosen and regrown from scratch using the configurational bias Monte Carlo approach.[27−29] The new regrown chain is then accepted with the Rosenbluth acceptance criterion

$$p_{acc} = \min\left[1, \frac{W_{new}}{W_{old}}\right] \quad (7)$$

where W_{old} and W_{new} are the Rosenbluth weights corresponding to deleting the chain and regrowing a new one, respectively. Both moves are fairly standard and satisfy the detailed-balance condition.

The PMF, $A(d)$, is computed by integrating the computed force as follows:

$$A(d) = -\int_{\infty}^{d} \langle F(\xi)\rangle \, d\xi \quad (8)$$

Note that the PMF is denoted by the symbol A, as it is essentially a Hemholtz free energy. $A(d)$ can be further divided into energetic and entropic contributions to determine their relative importance in governing colloidal interactions. The energetic component can be computed as

$$U(d) = \int \ldots \int U_{tot}(d, \mathbf{\Omega}) \exp(-U_{tot}(d, \mathbf{\Omega})/k_B T) \, d\mathbf{\Omega} \quad (9)$$

Note that the same Monte Carlo simulation used for computing the averaged force and PMF can be used for computing $U(d)$. The entropic contribution $S(d)$ can then be computed as follows:

$$S(d) = \frac{U(d) - A(d)}{T} \quad (10)$$

The PMFs have been computed for different values of surface and polyelectrolyte charges by changing q_c and q_p independently in the range $0-\pm 2.4e$. Note that many of these combinations do not yield overall electroneutral systems. Other parameters such as colloid size, chain length, temperature, and salt concentration are kept constant throughout this study (see Table 1 for a complete list). An exhaustive study of the role of all parameters is beyond the scope of this study due to the computational demands; the current study alone involved about 10 000 h of CPU time on 3.2 GHz Intel EM64T processors. However, we believe that the main conclusions drawn from this restricted parameter space are sufficiently general.

3. Results and Discussion

3.1. Potential of Mean Forces. We have used the above MC methodology to compute the PMF between two colloidal particles for different combinations of surface and polyelectrolyte charges. Figure 2 shows four representative PMF profiles plotted for different colloid surface and polyelectrolyte charge values: $(q_c, q_p) = (0.5e, -0.5e)$, $(1.0e, -1.0e)$, $(1.5e, -1.5e)$, and $(1.0e, -2.5e)$. The force profile $\langle F(d)\rangle$ from which the PMFs were computed are shown for reference. We have also plotted the relative contributions of energy $U(d) - U(\infty)$ and entropy $TS(d)$. Note that the energetic contribution to the PMF has been plotted as the total energy of the system relative to its value when the two colloidal particles are an infinite distance apart. The latter is calculated separately as 2 times the total energy of a single isolated colloidal particle.

The PMF profiles exhibit a strong dependence on both the surface and polyelectrolyte charges. Interestingly, some PMF profiles become negative within a range of separation distances (Figure 2b,c), suggesting an effective attraction between the colloidal particles, while others remain positive over the entire separation distance range (Figure 2a,d), indicating repulsion. Interestingly, in some PMFs, the entropy term contributes more than the energy toward the net attraction (see, for example, Figure 2c). The PMF profiles also exhibit common features irrespective of the two charges such as the sharp repulsion observed at short distances and the slowly decaying repulsion at large separation distances. The former arises from the chain overlap (to be discussed in more detail later) and overlap in the excluded volume of surface charges, and the long-range repulsion arises from the colloidal particles behaving like point charges of the same sign and magnitude at large separation distances.

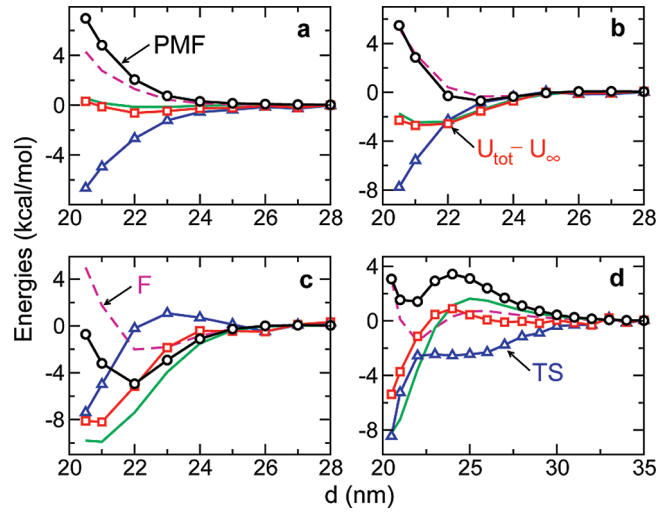

Figure 2. Potential of mean force (A) (black circes), total energy (U) (red squares), and entropy (TS) (blue triangles) profiles at different colloid surface and polyelectrolyte charge combinations (q_c, q_p): (a) $(0.5e, -0.5e)$, (b) $(1e, -1e)$, (c) $(1.5e, -1.5e)$, and (d) $(1e, -2.5e)$. Also shown are the force profiles (F) (dashed magenta lines).

3.2. Hyperbolic Attractive Regime. To determine the extent of the observed attraction in q_c-q_p charge space, we have categorized the PMFs as *attractive* when they fall negative, usually for a short range of distances only (e.g., Figure 2b,c), and *repulsive* when the entire PMF is positive (e.g., Figure 2a,d). Figure 3a shows the attractive and repulsive regimes for our colloidal system. The dashed curve represents a hypothetical boundary separating the two regimes. Intriguingly, the boundary exhibits a hyperbolic shape, with the attractive regime occupying the inner portion of the hyperbola with the repulsive regime on the outside. The hyperbola does not extend all the way to the origin, as there appears to be some repulsion at small q_c and q_p. The hyperbola also seems to be symmetrically arranged on the q_c-q_p plane; i.e., its major axis tilts close to the electoneutrality condition indicated by the dashed line in the figure. We have explored other chain flexibilities and grafting densities, and our preliminary results suggest that the hyperbolic shape of the boundary may be universal.

The computed PMF profiles can also be used to estimate the stability of the colloids under dilute conditions. Essentially, this involves computation of the osmotic second virial coefficient via the McMillan−Mayer expression:[30]

$$B_2 = 2\pi \int_{2R}^{\infty} [1 - \exp(-A(r)/k_B T)] r^2 \, dr \quad (11)$$

where r is the separation distance between two colloidal particles. A positive value of B_2 is generally indicative of a stable

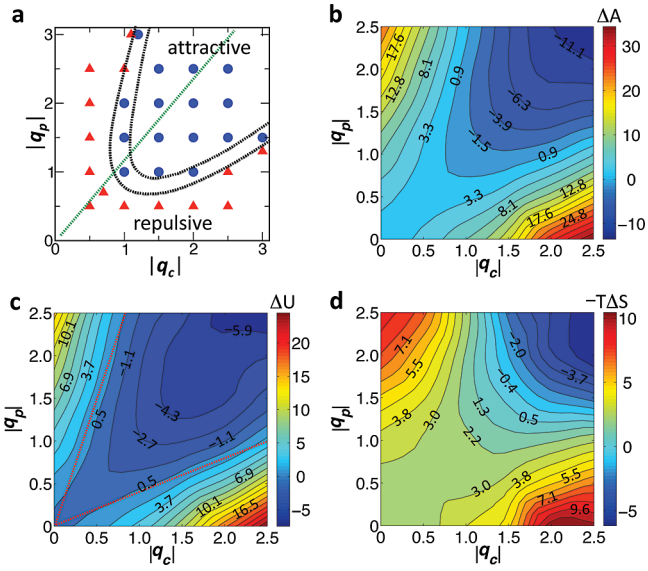

Figure 3. (a) Attractive and repulsive regimes for polyelectrolyte-grafted colloids in the q_c-q_p space. Blue circles and red triangles represent attractive and purely repulsive PMFs at the specified surface and polyelectrolyte charges, respectively. The dashed black line represents the hypothetical boundary between the attractive and repulsive regimes. The dot−dashed line corresponds to the rough stability limit obtained from the second virial coefficient. The green dashed line represents the electroneutrality condition. (b−d) Contour plots for the change in (b) free energy (ΔA), (c) energy (ΔU), and (d) entropy ($-T\Delta S$) when two colloidal particles are brought from infinity ($d = \infty$) to a separation distance of $d = 22$ nm in the q_c-q_p space. Values for a few selected contours are shown in each plot. The red dashed lines in part c correspond to the upper and lower bound of the negative-energy region predicted by our phenomenological model (eq 14).

system, while negative values generally imply susceptibility to phase separation and crystallization. We have computed B_2 using the above equation for all charge conditions and plotted the boundary between positive and negative values of B_2 as the dot−dashed curve (inner hyperbola) in Figure 3a. This boundary represents a more stringent condition for attraction between colloids, as it accounts for thermal effects; i.e., the PMF does not need to be necessarily positive for the colloids to be stable, as very weakly attractive PMFs can also be stable under thermal fluctuations.

To understand the origin of attraction between colloidal particles and the mechanisms that give rise to the hyperbolic shape of the attractive regime, we have decomposed the PMF into energetic and entropic contributions using eqs 9 and 10. In Figure 3b−d, we have plotted the contour maps of the computed PMF, and energetic and entropic contributions in the q_c-q_p space using the MATLAB routine *contourf*. We have chosen these quantities to be computed at a colloid separation distance of $d = 22$ nm at which several PMFs exhibit a minima (see Figure 2). Note that the contour lines representing the zero PMF value in Figure 3b may be slightly different from the attractive−repulsive boundary plotted in Figure 3a, as the former only consider the value of the PMF at $d = 22$ nm while the latter searches along the entire range $d > 20$ nm to assess if the PMF is attractive or repulsive.

Clearly, the attraction between the colloids is dictated by a complex interplay between energy and entropy, each of which depends strongly on the surface and polyelectrolyte charge. Next, we examine these two components of the total free energy in more detail and provide phenomelogical models to explain their charge dependence and contribution to this net attraction.

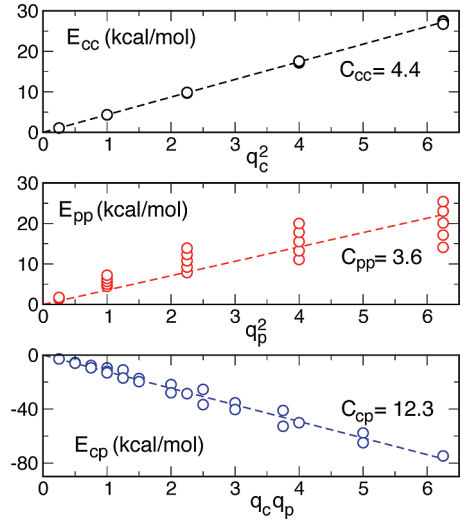

Figure 4. Linear regression of various energetic components with respect to surface and polyelectrolyte charge: (a) core−core repulsion (E_{cc}) with q_c^2; (b) polyelectrolyte−polyelectrolyte repulsion (E_{pp}) with q_p^2; (c) surface−polyelectrolyte attraction (E_{cp}) with $q_c q_p$. The values of proportionality constants (line slopes) obtained from the regression are also provided.

3.3. Energetic Contribution to Attraction. The energy contours in Figure 3c indicate that the favorable (negative) energies fall within a triangular region in the q_c-q_p space whose lower and upper bounds converge at the origin ($q_c = q_p = 0$). In particular, the most negative energies occur at $(q_c, q_p) = (2.5e, -2.5e)$ ($\Delta U \approx -6$ kcal/mol) and some of the most unfavorable energies occur at $(q_c, q_p) = (2.5e, 0e)$ ($\Delta U \approx 24$ kcal/mol) and $(q_c, q_p) = (0e, -2.5e)$ ($\Delta U \approx 15$ kcal/mol). This behavior may be explained by considering that the total energy of the system is given by the sum of electrostatic energy, chain stretching and bending energy, and van der Waals energy. As the particles are brought closer, the net change in the energy, ΔU, is dominated by an increase in the surface/surface and chain/chain electrostatic repulsion and an increase in the surface/chain electrostatic attraction. The chain stretching and bending and van der Waals energies do not change significantly until the surface charges on apposing colloids begin to overlap (i.e., $d \rightarrow 2R$). When $|q_c| \gg |q_p|$ or $|q_c| \ll |q_p|$, the repulsion terms dominate the attractive interactions, making the total energy positive. As q_c and q_p become comparable, the attractive terms begin to dominate, causing the total energy to be negative and attractive.

A rough model may be formulated to capture this behavior. For this purpose, we have computed for different combinations of q_c and q_p the repulsive energy between the two colloid surfaces (E_{cc}) and between the two grafted polyelectrolyte layers (E_{pp}) and the attractive energy between the surface and polyelectrolyte chains (E_{cp}). In Figure 4, we have plotted E_{cc}, E_{pp}, and E_{cp} as a function of q_c^2, q_p^2, and $|q_c q_p|$, respectively. Though the electrostatic energy between two point charges is directly proportional to the product of the two charges, we do not expect the proportionality to hold for the ensemble averages E_{pp}, E_{cp}, and E_{pp} due to the nature of the Boltzmann averaging. Regardless, the energies still vary roughly linearly with their respective charge products, with E_{cc} and E_{cp} exhibiting the strongest linear dependence (Figure 4a,c). Noting this linear dependence, we propose that the energy change as two particles are brought from infinity to a distance d (=22 nm) is given by

$$\Delta U \simeq C_{cc}q_c^2 + C_{pp}q_p^2 - C_{cp}|q_c||q_p| \qquad (12)$$

where the first two terms represent the electrostatic repulsion between the surfaces and chains, respectively, and the third term represents the electrostatic attraction between the surface and chains. The coefficients C_{cc}, C_{pp}, and C_{cp} are all positive, and may be obtained through a linear fit of the energies, as shown in Figure 4. It can now be easily shown (by equating eq 12 to zero) that the negative-energy regime falls within

$$\left(\frac{C_{cp} - \sqrt{C_{cp}^2 - 4C_{cc}C_{pp}}}{2C_{pp}}\right)|q_c| < |q_p| < \left(\frac{C_{cp} + \sqrt{C_{cp}^2 - 4C_{cc}C_{pp}}}{2C_{pp}}\right)|q_c| \qquad (13)$$

The linear fits in Figure 4 yield $C_{cc} = 4.36$, $C_{pp} = 3.55$, and $C_{cp} = 12.29$, yielding $|q_p| = 3.1|q_c|$ and $|q_p| = 0.4|q_c|$ as the upper and lower bounds of the negative-energy region, respectively (see Figure 3c). Hence, this crude phenomenological model can explain the observed triangular nature of the negative-energy regime in the $q_c - q_p$ plot.

We further dissect E_{pp} and E_{cp} into its intra- and interparticle contributions: repulsion energy arising from chains of the same particle (E_{pp1}) and of different particles (E_{pp2}) and attraction energy between the colloid surface and its own chains (E_{cp1}) and those of the other colloid (E_{cp2}). These contributions along with E_{cc} have been plotted as a function of distance d for a representative overall attractive system at $q_c = -q_p = 1.5e$ (also used in Figure 2c). Expectedly, E_{cc} and E_{pp2} increase monotonically as the particles approach each other, with the former exhibiting more short-ranged repulsion. The approach also causes E_{pp1} to increase monotonically due to compression of the chains. The intra- and interparticle attraction energies exhibit a more interesting interplay: E_{cp2} decreases monotonically as the particles approach, while E_{cp1} increases with approach until $d = 22$ nm and then exhibits a small decrease thereafter. This suggests that some of the chains adsorbed on the surface of the colloid contributing to E_{cp1} detach and adsorb onto the surface of the other colloid as the two particles approach each other.

We next extricate the contribution of polymer bridging to the attraction E_{cp2} from that due to the "cloud" of chains around one colloid interacting remotely with the surface of another particle. We define the polymer-bridging energy as the electrostatic energy between polyelectrolyte beads of one colloid and the surface charges of the other when the two are within 2 nm of each other; the variation of this energy with interparticle distance is plotted in Figure 5. Though it may seem that polymer bridging contributes only ~18% to the attraction E_{cp2} at $d =$ 22 nm, it is quite significant given that it is comparable to the net attraction between the particles (ΔA). We find that polymer-bridging interactions consistently contribute ~15−18% to E_{cp2} when the surface and chain charges are comparable but their contribution decreases as the two charges become dissimilar. Hence, polymer-bridging interactions do contribute significantly to the overall attraction observed between the colloidal particles.

3.4. Entropic Contribution to Attraction. We now turn our attention to the entropy contours in Figure 3d, which exhibit a more complex charge dependence than the energy. At small magnitudes of q_c and q_p, there is a moderate loss in the entropy [$T\Delta S \approx -2$ kcal/mol at $(q_c, q_p) = (0.5e, -0.5e)$]. As q_c is increased keeping q_p fixed, and vice versa, the entropy loss

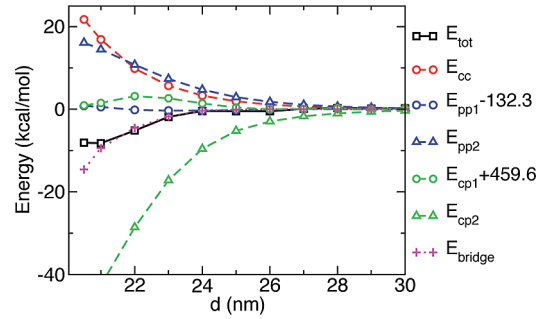

Figure 5. Variation of different energy components with interparticle distance: repulsion between charged surfaces (E_{cc}), repulsion between chains across different particles (E_{pp1}), repulsion between chains from different colloids (E_{pp2}), attraction between chains and surface within the same colloids (E_{cp1}), and attraction between chains and surface across different colloids (E_{cp2}). Also shown in the plot is the total energy E_{tot} and the energy contribution from bridging interactions E_{bridge}.

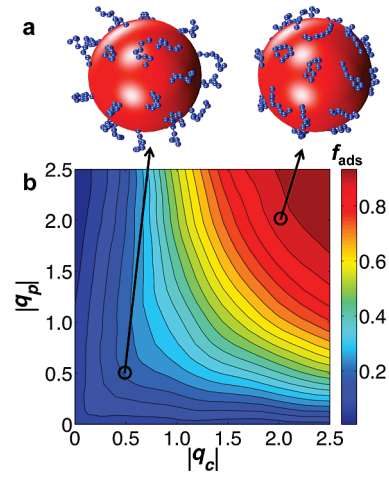

Figure 6. (a) Two representative snapshots of the colloidal particle at $(q_c, q_p) = (0.5e, -0.5e)$ (extended) and $(2.5e, -2.5e)$ (collapsed). (b) Contour plot showing the variation in the fraction of polyelectrolyte chains adsorbed at the surface of an isolated colloid (f_{ads}) with the colloid surface and polyelectrolyte charge.

becomes more severe such that, at $(q_c, q_p) = (0.5e, -2.5e)$ and $(2.5e, -0.5e)$, $T\Delta S \approx -6$ kcal/mol. However, a simultaneous increase in both q_c and q_p results in the opposite effect: the entropy change becomes smaller until it changes sign and becomes positive (favorable). In fact, at $(q_c, q_p) = (2.5e, -2.5e)$, the entropy gain is quite substantial ($T\Delta S \approx +6$ kcal/mol).

To understand this nontrivial dependence of entropy on the charges, it is important to first note that the polyelectrolyte chains exhibit two types of conformations in isolated particles: collapsed, where the chains are strongly adsorbed onto the parental colloid surface, and extended, where the chains stretch outward into the solution (Figure 6a). In Figure 6b, we have plotted the fraction of strongly adsorbed chains (f_{ads}) in an isolated particle as a function of surface and polyelectrolyte charges; a chain is considered adsorbed when one or more of its three terminal beads remain within 1 nm of the surface. Clearly, the chains prefer to stay extended when the surface charge is small, and become increasingly adsorbed with an increase in their attraction to the surface, which scales roughly as the product of the two charges $|q_cq_p|$. It may therefore seem surprising that the chains become more extended with their charge for weakly charged surfaces even though the attraction between the chains and the surface increases. This difference can be explained on the basis that, as the chains become more charged, they also become stiffer due to repulsion between non-

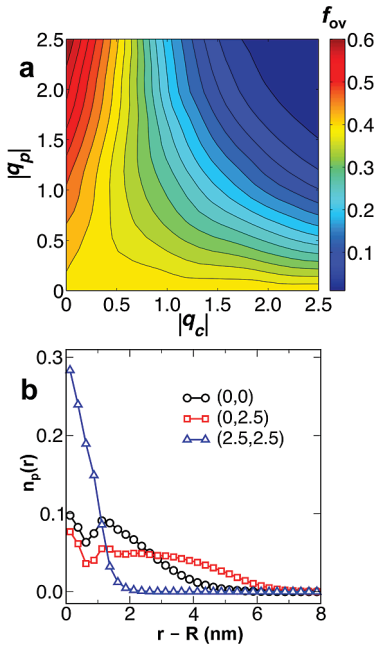

Figure 7. (a) Contour plot of the variation of the degree of overlapping polyelectrolyte overlap between two colloidal particles f_{ov} separated by a distance of $d = 22$ nm. (b) The density of polyelectrolyte chains $n_p \propto 4\pi r^2 \rho(r)$ as a function of normal distance from the colloid surface for $(q_c, q_p) = (0e, 0e)$ (black squares), $(0e, -2.5e)$ (red squares), and $(2.5e, -2.5e)$ (blue triangles).

neighboring beads, forcing them to adopt more extended conformations.

Three effects need to be considered to understand the origin of the complexity in the entropy landscape of Figure 3d. First, as the particles are brought closer, the chains confined between them begin to overlap and get squeezed, causing them to lose entropy. This "chain overlap" effect is the strongest when the chains adopt extended conformations and the weakest when the chains are strongly adsorbed. We have quantified this effect in Figure 7a by computing the fraction of chain beads (f_{ov}) that lie beyond a 1.5 nm shell around the colloidal surface and would get squeezed when a second particle is brought within a distance of 2 nm from its surface, as given by

$$f_{ov} = \frac{\int_{R+1.5}^{\infty} n_p(r)\, dr}{\int_{R}^{\infty} n_p(r)\, dr} \qquad (14)$$

where n_p is the number of chain beads inside a shell of unit thickness and radius r from the center of an isolated colloidal particle and is directly related to density $\rho(r)$ as $n_p(r) = 4\pi r^2 \rho(r)$. The variation of n_p with r for three charge combinations is plotted in Figure 7b. Note that we use 1.5 nm here rather than 2 nm to account for the excluded volume of the colloidal surface (surface charges). We note that the chains are most extended, and thereby lose the most entropy, when the colloid cores are uncharged or slightly charged and when the chains are strongly charged. The chains are in a collapsed state when both the surface and polyelectrolyte are strongly charged, and lose little entropy when particles are brought into close proximity. Hence, the contour plot for f_{ov} in Figure 7b "mirrors" that of f_{ads} (Figure 6b), as the two represent opposite effects.

Second, the chains could also lose entropy when two colloidal particles are brought closer by accumulating in the gap between

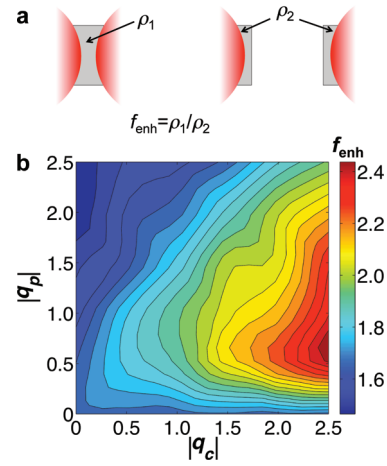

Figure 8. (a) Schematic showing the computation of density enhacement f_{enh}. (b) Contour plot showing density enhancement f_{enh} of polyelectrolyte chains confined between colloidal particles $d = 22$ nm apart as a function of colloid surface and polyelectrolyte charge.

the particles. Such "density enhancement" results from the favorable electrostatic potential inside the gap and at the surfaces and from the reduction in the free volume available to the chains as the particles are brought closer. We characterize density enhancement in terms of the quantity f_{enh}, which represents the ratio of the average chain density within a cylindrical volume of radius $r = 4.5$ nm confined between colloids separated by a distance of $d = 22$ nm (minus the volume of the two spherical caps which excludes the chains) and the average chain density within a cylindrical volume of the same radius but half the length (minus the volume of one spherical cap) when the two particles are far apart (see Figure 8a). The density is calculated as the number of polyelectrolyte beads present per unit volume. Hence, $f_{enh} > 1$ implies that the chain density is higher in between the particles compared to outside, leading to a reduction in chain entropy. Note that $f_{enh} = 2$ in an idealized scenario where chains do not interact with each other; excluded volume and repulsive interactions are expected to decrease f_{enh} below this value, and attractive interactions between chains and the apposing surface are expected to increase f_{enh}. The computed f_{enh} values for our colloids are shown as a contour plot in Figure 8b. Clearly, f_{enh} exhibits a strong modulation with the surface and polyelectrolyte charges: it is large (>2) for strong surface and weak polyelectrolyte charges and small (<2) for the opposite condition. Hence, the stronger the repulsion between the chains, the lesser is the chain density between the colloids.

This effect is also clearly visible from the chain density contour plots of Figure 9, where more than 2-fold enhancement in the density is observed for $(q_c, q_p) = (2.5e, -0.5e)$ and $(2.5e, -2.5e)$ when the two colloidal particles are near compared to far. The plots have been constructed by computing the chain density along planar slices of thickness 1 nm passing through the centers of two colloids placed $d = 22$ nm apart, and averaging this density over an ensemble of such slices oriented at different angles within a $[0, \pi]$ range.

Interestingly, the third effect, which we call "chain flipping", leads to entropy *gain* when two colloidal particles are brought in close proximity. When particles get close, it allows the chains adsorbed on the surface of one colloid to detach and adsorb onto the surface of the apposing colloid, allowing chains to sample two potential energy minima, as depicted schematically in Figure 10a. Such a mechanism leads to reasonably large gains in chain entropy. We expect this effect to be prominent for chains strongly adsorbed at their parent colloid that possess little

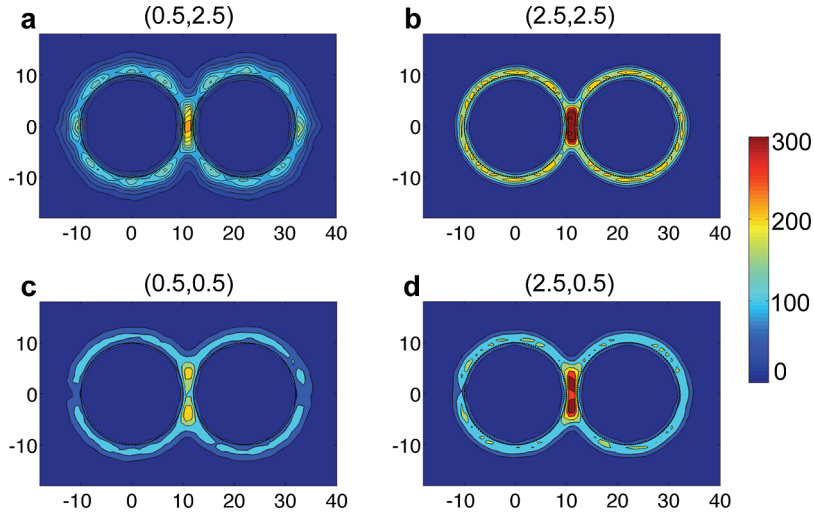

Figure 9. Contour plots of the polyelectrolyte density for colloidal particles separated by a distance of $d = 22$ nm at four different combinations of surface and polyelectrolyte charges (q_c, q_p): (a) (0.5e, −2.5e), (b) (2.5e, −2.5e), (c) (0.5e, −0.5e), and (d) (2.5e, −0.5e). The scale is arbitrary.

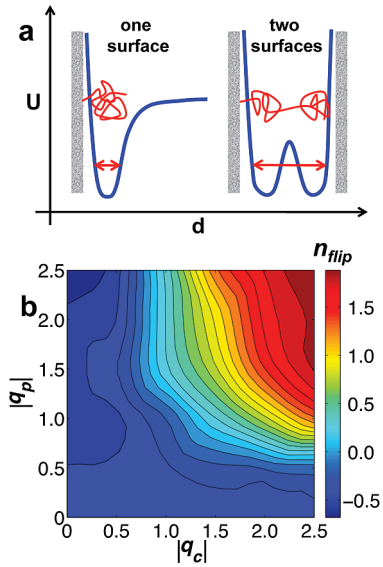

Figure 10. (a) Schematic explaining the increase in the entropy of strongly adsorbed chains when two colloidal particles are brought closer. The blue curve depicts a cartoon of the potential energy, and the red squiggle represents the grafted polymer. (b) Contour plot showing the number of polyelectrolyte chains that switch from adsorbing at the surface of their parent to adsorbing at the surface of the second colloid, n_{flip}.

entropy to begin with, such as those associated with strongly charged surfaces. This effect may also be roughly quantified in terms of the number of chains switching from the parent surface to the apposing surface, n_{flip}, when two particles are brought from infinity to a distance of $d = 22$ nm. A rough calculation assuming that the number of possible configurations of the polyelectrolyte doubles through this flipping mechanism estimates an entropy gain of $k_BT \ln 2$ (∼0.42 kcal/mol) per chain. Figure 9b plots the contour maps of n_{flip} on the q_c−q_p space. Clearly, the mechanism is most prevalent when both q_c and q_p are large, i.e., when most of the chains are adsorbed strongly onto the surface of their colloids and negligible when the chains prefer to extend outward.

We can now explain the complex charge dependence of the entropy change observed in Figure 3d in terms of the three mechanisms of entropy change discussed above. We focus on the four corner regions of the plot for convenience. When both q_c and q_p are small, we observe a moderate loss in entropy. This loss occurs primarily due to chain overlap, as the chains are well-extended in this regime and lose significant entropy when the particles approach each other (see Figure 7). The other two mechanisms, chain enhancement and chain flipping, do not contribute to the entropy change due to the weak surface charge and minimal chain adsorption, respectively. Chain overlap is also responsible for the sharp reduction in total entropy observed at small separation distances of $d < 22$ nm (Figure 2). When both q_c and q_p are large, the overall entropy change is favorable. Here, the chains are strongly adsorbed at the surface and gain significant entropic freedom when a second charged surface allows the chains to explore both surfaces (see Figure 10). The entropy loss due to chain enhancement and overlap is small in this regime. When q_c is large but q_p is small, the entropy reduction is dominated by chain enhancement; i.e., the chains accumulate in the region between the two particles due to their strongly charged surfaces, leading to limited freedom (Figure 8). The entropy changes due to chain flipping and chain overlap are weak in this regime. Finally, in the regime of small q_c and large q_p, the chains are stretched outward and lose significant entropy when they overlap with the chains from a proximal particle (Figure 10). The effects from chain density enhancement and chain flipping remain weak, as the colloid surfaces are weakly charged. Hence, the complex dependence of entropy on the colloid surface and polyelectrolyte charge strength may easily be explained as a convolution of three charge-dependent mechanisms of entropy change.

3.5. Charge Dependence of Total Free Energy. Figure 3b shows a contour plot of the change in the free energy (ΔA or PMF) when two colloidal particles are brought from infinity to close proximity ($d = 22$ nm) as a function of the colloid surface and polyelectrolyte charge. The particles are repulsive when both the surface and polyelectrolyte chains are weakly charged ($\Delta A \approx 3.5$ kcal/mol when q_c, $q_p \rightarrow 0$) and become extremely repulsive when one of the charges (surface or polyelectrolyte) is much larger than the other (e.g., $\Delta A \approx 34$ kcal/mol when $q_c = 2.5e$ and $q_p = 0$). However, when both charges are increased simultaneously, the particles begin to exhibit net attraction such that, at $q_c = 2.5e$ and $q_p = -2.5e$, the particles are extremely attractive with $\Delta A \approx -11$ kcal/mol.

These trends can be explained in terms of changes in energy and entropy. At small q_c and q_p, the energetic changes are favorable but the unfavorable entropic changes dominate,

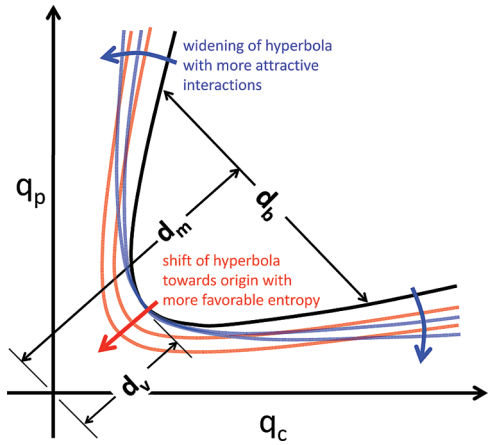

Figure 11. Schematic showing how the phenomenological model (eqs 16 and 17) predicts that the hyperbolic attractive regime would expand and translate depending on the ratio of attractive to repulsive interactions and the strength of entropic interactions, respectively.

making the overall PMF positive and the particles repulsive. The particles become even more repulsive when q_c is small and q_p is large (or vice versa), as both the energetic and entropic changes are now unfavorable. When both q_c and q_p are large, both the energetic and entropic changes contribute favorably in making the colloidal particles attractive. The net result of such an interplay between energetic and entropic factors is a hyperbola-shaped boundary separating the attractive and repulsive regimes (Figure 3).

The hyperbolic shape of the attractive regime boundary may be explained by extending the phenomenological model that we proposed earlier to explain the triangular negative-energy regime. Our previous model (eq 12) accounted for energy changes in bringing two particles close to each other. We now add an entropic term to this model; this is however not a trivial task, as the charge dependence of the entropy is quite complex. To this end, we make the simplified approximation that the entropy loss is described by a constant $\Delta S_0 < 0$ based on the observations that the entropy change is negative in the low charge regime and that the charge dependence of the entropy change in this regime is weak. The total free energy of the two-colloid system therefore simply becomes

$$\Delta A \simeq C_{cc}q_c^2 + C_{pp}q_p^2 - C_{cp}|q_c||q_p| - T\Delta S_0 \quad (15)$$

The boundary of the attractive regime may now simply be obtained by setting ΔA to zero, which indeed yields the standard equation of a hyperbola.

Next, we explore some properties of this hyperbola to predict roughly how changes in energetic and entropic terms affect the shape and location of the attractive regime. To facilitate such an analysis, we exploit the symmetric shape of the hyperbolic regime in the q_c-q_p space and suggest that $C_{cc} \sim C_{pp}$. It can now be shown that the distance of the vertex of the hyperbola (intersection of the hyperbola with its major axis; Figure 11) from the origin is given by

$$d_v = \sqrt{\frac{-T\Delta S_0}{C_{cp}/2C_{cc} - 1}} \quad (16)$$

and the breadth of the hyperbola at a distance d_m from the origin is given by

$$d_b = 2d_m\sqrt{\frac{C_{cp} - 2C_{cc}}{C_{cp} + 2C_{cc}}} \quad (17)$$

where $C_{cp} > 2C_{cc}$ for an attraction to exist. Equation 16 suggests that the attractive regime should shift away from the origin (d_v increases) when either the entropic penalty becomes larger, i.e., $-T\Delta S_0$ increases, or the attractive polymer/surface interactions become weak, i.e., $C_{cp} \rightarrow 2C_{cc}$ (Figure 11). Equation 17 suggests that the breadth of the attractive regime, d_b, should increase as the attractive terms in the energy (polymer-bridging interactions) dominate the repulsion of the surfaces and the chain, i.e, $C_{cp} \gg 2C_{cc}$. Both predictions look reasonable, and it would be interesting to test them through additional simulations and experiments. Also, a more rigorous quantitiative model invoking proper averaging of repulsive and attractive interactions in eq 5 would be highly useful.

3.6. Implications. An important result of this study is that the entropy plays an equally important role as energy in dictating the strength of attraction between polyelectrolyte-grafted colloids. On the one hand, it promotes repulsion for weakly charged particles (q_c and q_p small), but on the other hand, it promotes attraction for strongly charged colloids (q_c and q_p large). Since the entropic interactions are dictated by a competition between chain adsorption at the surface of the colloid and their bridging across two colloidal particles, it would be interesting to test if this dual role of entropy can be modulated by changing the flexibility of the polyelectrolyte chains or their attachment configuration at the surface.

Another key result is the characteristic hyperbolic shape of the attractive regime. The shape and inclination of this hyperbola relative to q_c and q_p axes imply two general trends. First, the magnitude of the attractive force follows a nonmonotonic dependence with charge when either the surface or polyelectrolyte charge is increased while keeping the other charge constant. Second, the attractive force increases monotonically when the surface and polyelectrolyte charges are increased simultaneously. These trends now explain why previous studies examining a very narrow range of charge space sometimes observed a monotonic increase in the attraction between colloids with the surface charge[19] while other times a nonmonotonic dependence with surface charge was observed.[12,21]

Our results also provide basis for the observation that polyelectrolyte-grafted colloids exhibit a very rich phase behavior. Also, our study suggests that the phase properties of such colloidal systems could be controlled through manipulation of the surface and/or polyelectrolyte charge. As an example, consider a stable colloidal system in which the surface and polyelectrolyte charges differ significantly in magnitude to promote repulsion among particles. One can envision that such a system could be forced to phase separate (destabilize) by simply changing the solution pH in order to make the surface and polyelectrolyte charges more comparable in magnitude through selective protonation or deprotonation of their chemical groups.

It should also be emphasized that our model system represents only a small subset of the available parameter space. Some of the other parameters whose effects are not studied here include chain flexibility and length, grafting density, temperature, and salt concentration. Though changes in these parameters could certainly affect the magnitude of the energetic and entropic forces, we believe the qualitative interplay between them to produce hyperbolic regions of attraction will remain unchanged. For example, in this study, the van der Waals energy parameter

has been deliberately kept small to focus on the electrostatic contributions, but we expect that these van der Waals interactions could potentially contribute to long-range attraction scaling as $\sim d^{-2}$ in the case of spherical colloids.[31] On the basis of our results (Figure 11), we expect such longer-ranged attraction that is independent of charge values to bring the attractive regime closer to the origin in the q_c-q_p plot.

It is also instructive to analyze the physical relevance of the charge values examined in this study. We have considered a maximum charge of 2.5*e* on each polyelectrolyte bead of size 1 nm, which translates to a line-charge density of 3.0*e*/nm. Single-stranded and double-stranded DNA that are often tethered to colloids have line-charge densities of 3 and 6*e*/nm, respectively. If these densities are calculated on the basis of the actual extension of DNA, they turn out to be even higher. Further, the highest surface charge values considered in this study are 3.0*e* corresponding to a charge density of $\sim 0.7e/\text{nm}^2$, which is well within the reach of biological membranes[32] and nanoparticles.[33] Hence, both our polyelectrolyte and colloid charges are within reasonable physical bounds.

Finally, an issue that this study does not fully address is the role of charge correlations in the observed attraction between colloidal particles. Generally, charge correlations are important when the charges are multivalent and/or the charge densities are high. Hence, one expects this effect could be important when our polyelectrolyte chains becomes strongly charged. However, we believe that charge correlations may not be very important for our system, as compared to polymer-bridging interactions, based on two recent findings. Muhlbacher et al.[7] studied a system similar to ours to show that the net attraction between particles decays in a manner consistent with polymer-bridging mediated attraction rather than charge-correlation mediated attraction which decays with a characteristic Debye length. In another study, Turesson et al.[23] used a special Poisson−Boltzmann theory to demonstrate that charge correlations dominate attraction only in the limit of stiff chains where the entropic cost of forming bridges across surfaces becomes formidable. Given that the attraction observed in our colloids persists for distances longer than the Debye length (2 nm) and that our chains are fairly flexible, we do not anticipate that charge correlation is very significant in our study.

4. Conclusions

In this paper, we provide new insights into the attraction between polymer-grafted colloidal particles, where the surface of the colloid and the polymer chains carry opposite charges. We employ Monte Carlo simulations to compute the potential of mean force (PMF) between two such colloidal particles treated at the coarse-grained level as a function of their separation distance. The computed PMFs display a rich behavior with respect to the charges carried by the surface and polyelectrolyte chains, with some PMFs showing attractive forces and others showing purely repulsive interactions. By categorizing the PMFs as attractive or repulsive, we obtain the extent of the attractive-force regime of the colloids in the two-dimensional space of the surface and polyelectrolyte charge. We find that the boundary of the attractive regime exhibits a characteristic hyperbolic shape, where the attractive regime occupies the inside of the hyperbola and the repulsive regime occupies the region outside.

To provide further insights, we have decomposed the PMF into its energetic and entropic contributions. We observe that a complex interplay between energetic and entropic factors dictates the attraction between colloidal particles. In general, the energy of the system is dictated by a competition between the energy loss from polymer/surface interactions, which includes polymer-bridging interactions, and the energy gain from mutual repulsion between the surfaces and the polyelectrolyte chains. The entropy is dictated by several factors: favorable entropy gain from polyelectrolyte chains flipping between the two colloid surfaces, associated with polymer-bridging, and entropy loss due to overlap of polyelectrolyte chains and their accumulation in the electrostatically favorable region in between the particles. For particles with weakly charged surfaces and polyelectrolyte chains, the entropy loss arising from chain overlap dominates the favorable polymer/surface interactions, resulting in a net repulsion. When both the surface and polyelectrolyte chains are strongly charged, the energy loss due to polymer/surface interactions and the entropic gain from chain flipping contribute to net attraction between particles. When one of the charges (surface or polyelectrolyte) dominates the other, strong repulsive forces arise due to a combination of severe repulsion between the surfaces and large entropy loss due to chain overlap and accumulation in the region confined between two particles.

The result of this interplay is a hyperbola-shaped region of attraction in the two-dimensional charge space. We propose a rough phenomenological model to explain this particular shape of the attractive regime and to make useful predictions regarding its size and location with respect to changes in energetic and entropic interactions. Our results also explain past discrepancies in experimental results concerning the charge dependence of attractive forces and suggest ways of controlling the interaction between polymer-grafted colloidal particles through charge modulation.

Acknowledgment. G.A. acknowledges computer time on the Granite supercomputing cluster of the Bioengineering Department at UCSD and thanks Prof. Bo Li for discussions and Jun Park for performing some simulations.

References and Notes

(1) Taylor, K. C. *J. Pet. Sci. Eng.* **1998**, *19*, 265–280.
(2) Forsman, J. *Curr. Opin. Colloid Interface Sci.* **2006**, *11*, 290–294.
(3) Podgornik, R.; Licer, M. *Curr. Opin. Colloid Interface Sci.* **2006**, *11*, 273–279.
(4) Bertin, A.; Leforestier, A.; Durand, D.; Livolant, F. *Biochemistry* **2004**, *43*, 4773–4780.
(5) Mangenot, S.; Leforestier, A.; Durand, D.; Livolant, F. *J. Mol. Biol.* **2003**, *333*, 907–916.
(6) Arya, G.; Schlick, T. *Proc. Natl. Acad. Sci. U.S.A.* **2006**, *103*, 16236–16241.
(7) Mühlbacher, F.; Schiessel, H.; Holm, C. *Phys. Rev. E* **2006**, *74*, 031919.
(8) Black, A. P.; Birkner, F. B.; Morgan, J. J. *J. Colloid Interface Sci.* **1966**, *21*, 626–648.
(9) Edwards, S. F. *Proc. R. Soc.* **1965**, *85*, 613–624.
(10) deGennes, P. G. *Rep. Prog. Phys.* **1969**, *32*, 187–205.
(11) van Opheusden, J. H. J. *J. Phys. A: Math. Gen.* **1988**, *21*, 2739–2751.
(12) Podgornik, R. *J. Phys. Chem.* **1992**, *96*, 884–901.
(13) Borukhov, I.; Andelman, D.; Orland, H. *J. Phys. Chem. B* **1999**, *103*, 5042–5057.
(14) Huang, H.; Ruckenstein, E. *Adv. Colloid Interface Sci.* **2004**, *112*, 37–47.
(15) Podgornik, R. *J. Chem. Phys.* **2003**, *118*, 11286–11296.
(16) Huang, H.; Ruckenstein, E. *Langmuir* **2006**, *22*, 3174–3179.
(17) Podgornik, R.; Saslow, W. M. *J. Chem. Phys.* **2005**, *122*, 204902.
(18) Åkesson, T.; Woodward, C.; Jöhnsson, B. *J. Chem. Phys.* **1989**, *91*, 2461–2469.
(19) Miklavic, S. J.; Woodward, C. E.; Jönsson, B.; Åkesson, T. *Macromolecules* **1990**, *23*, 4149–4157.
(20) Sjöstrom, L.; Åkesson, T. *J. Colloid Interface Sci.* **1996**, *181*, 645–653.
(21) Granfeldt, M. K.; Jönsson, B.; Woodward, C. E. *J. Phys. Chem.* **1991**, *95*, 4819–4826.

(22) Dzubiella, J.; Moriera, A. G.; Pincus, P. A. *Macromolecules* **2003**, *36*, 1741–1752.
(23) Turesson, M.; Forsman, J.; Åkesson, T. *Langmuir* **2006**, *22*, 5734–5741.
(24) Korolev, N.; Lyubartsev, A. P.; Nordenskiöld, L. *Biophys. J.* **2006**, *90*, 4305–4316.
(25) Marsaglia, G. *Ann. Math. Stat.* **1972**, *43*, 645–646.
(26) Debye, P. W; Hückel, E. *Phys. Z.* **1923**, *24*, 185–206.
(27) Siepmann, J. I.; Frenkel, D. *Mol. Phys.* **1992**, *75*, 59–70.
(28) Frenkel, D.; Mooij, G. C. A. M.; Smit, B. *J. Phys.: Condens. Matter* **1992**, *4*, 3053–3076.
(29) de Pablo, J. J.; Laso, M.; Suter, U. W. *J. Chem. Phys.* **1992**, *96*, 2395–2403.
(30) McMillan, W. G.; Mayer, J. E. *J. Chem. Phys.* **1954**, *13*, 276–290.
(31) Israelachvili, J. *Intermolecular Surface Forces*; Academic Press: Oxford, U.K., 1991.
(32) Wiese, A.; Münstermann, M.; Gutsmann, B.; Lindner, B.; Kawahara, K.; Zähringer, U.; Seydel, U. *J. Membr. Biol.* **1998**, *162*, 127–138.
(33) Lucas, T.; Durand-Vidal, S.; Dubois, E.; Chevalet, J.; Turq, P. *J. Phys. Chem. C* **2007**, *111*, 18564–18576.

JP908007Z